Airfoil Transition and Separation Studies Using an Infrared Imaging System

Ehud Gartenberg* and A. Sidney Roberts Jr.†
Old Dominion University, Norfolk, Virginia 23508

An infrared imaging system was used to detect the thermal signature of boundary-layer flow regimes on a NACA 0012 airfoil from zero angle of attack up to separation. The boundary-layer transition from laminar to turbulent flow and the onset of separation could be seen on the airfoil thermograms. The findings were compared against the behavior of aluminum foil tufts observable both visually and with the infrared imaging system. This arrangement offers the option of using the infrared imaging system both for flow regime detection through surface thermography and flow visualization by the aluminum foil tufts. Ultimately the surface temperature changes due to variation in the angle of attack of a lifting surface provide a means for interpretation of the boundary-layer flow regimes.

Nomenclature

$c_{f,x}$ = local skin-friction coefficient
h_x = local heat transfer coefficient
k = air thermal conductivity
Nu_x = local Nusselt number
Pr = air Prandtl number
Re_x = local Reynolds number
St_x = local Stanton number
s = airfoil upper surface arc length
U = freestream air velocity
u = boundary-layer streamwise velocity component
x = chordwise coordinate
y = direction perpendicular to the airfoil surface
α = angle of attack
ν = air kinematic viscosity

Introduction

THE detection of boundary-layer transition from laminar to turbulent flow, or its separation from the surface of interest, remains a challenging subject. Many available experimental techniques are used for these studies: smoke visualization, laser Doppler velocimeters, tufts, chemical sublimation (acenaphtene), oil flow, hot films and hot wires, phase change paints, liquid crystal paints, pressure measurements, and optical techniques. Even so, the search for more rewarding techniques is ongoing. Infrared (IR) imaging systems have already been successfully used in the recent past to detect transition both in wind-tunnel and in flight testing.[1-6] However, the interpretation of separated-flow signature on IR thermograms is still an open subject, due to the difficulties associated with modeling and analysis of the heat transfer process in such regions. Therefore, it is interesting to see how the thermal signature of the various boundary-layer flow regimes on the surface of interest develops with the angle of attack. To help the thermogram interpretation, the flow behavior itself can be visualized by tufts observable with the IR imaging system, thus adding extra diagnostic capability to this tool while keeping the complexity of the experiment to the necessary minimum.

Received June 8, 1989; revision received July 11, 1990; accepted for publication July 11, 1990.

*Research Assistant Professor, Department of Mechanical Engineering and Mechanics. Senior Member AIAA.

†Professor, Department of Mechanical Engineering and Mechanics.

The observations to be reported refer to wind-tunnel experiments done on a NACA 0012 airfoil at a nominal chord Reynolds number of 375,000.

Boundary-Layer Behavior and the Thermal Surface Signature

To facilitate the understanding of the experimental results, a brief review is given about boundary-layer flows on the NACA 0012 airfoil at relevant Reynolds numbers (375,000), as the angle of attack is increased from zero up to separation.[7,8] The discussion is illustrated in Fig. 1 and is relevant to airfoils with a thickness ratio equal or greater than 12% (Ref. 8). At low angles of attack, the flow is laminar over a considerable part of the airfoil upper surface. Downstream from the peak suction point, the laminar boundary-layer separates with subsequent transition to turbulent flow. The expansion of the turbulent flow causes reattachment of the boundary layer as a turbulent one, which remains attached up to the trailing edge. The localized region of laminar separated flow is called the "laminar separation bubble." The air motion inside this bubble is circulatory, with typical velocities one order of magnitude lower than those in the freestream. The length of the bubble is a few percent of the chord. As the angle of attack is increased to moderate values, the bubble and the transition region above it move upstream, increasing the airfoil area subjected to turbulent flow. At a certain point, the turbulent boundary layer fails to negotiate the adverse pressure gradients, and part of it separates near the trailing edge. This phenomenon is known as turbulent separation. With the angle of attack increased to even higher values, the bubble moves further upstream, as does the point of turbulent separation, causing the influence of the angle of attack on the lift to decrease. Once the bubble reaches the leading edge, it stays attached to that area and remains small, while the separation

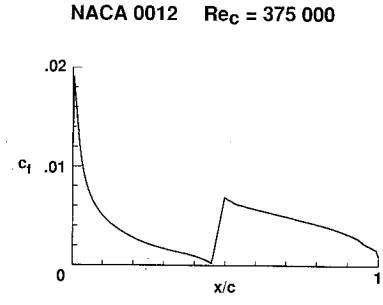

Fig. 1 Typical behavior of friction coefficient over upper surface of NACA 0012 airfoil; Re_c = 375,000.

point of the turbulent boundary layer continuously moves upstream. At a certain angle of attack (stall angle), the adverse pressure gradient can reach values where reattachment of the turbulent boundary layer is no longer possible. This causes the bubble to burst over the entire surface of the airfoil from the leading to the trailing edge, causing what is known as "leading-edge bubble-bursting stall."

Transition detection by surface IR thermography can be based on one of two heat transfer phenomena associated with the laminar to turbulent boundary-layer transition.[9] The first approach is based on the increased value of boundary-layer recovery temperature in the turbulent relative to the laminar regime. In a thermally stable flow, that part of a wing exposed to the turbulent regime should exhibit a higher adiabatic wall temperature relative to the part exposed to the laminar flow. This method works well at high temperatures and Mach numbers. However, at temperatures close to ambient and at low Mach numbers where the airflow is incompressible, this approach looses part of its usefulness, the surface temperature increase being close to, or even below, the IR camera temperature resolution. The second approach exploits the higher value of the heat transfer coefficient, associated with turbulent relative to laminar boundary-layer flow. This approach, which was used in the present experiments, can be used when the freestream air temperature changes with time, as is the case in closed-circuit wind tunnels where the air is continuously heating up.

The simplest way to illustrate this method of transition detection by surface IR thermography is through the Reynolds analogy between the skin friction and heat transfer. For fully developed laminar boundary-layer flow over a flat plate, the analogy states that

$$St_x = \frac{Nu_x}{Re_x Pr} = \frac{c_{f,x}}{2} \tag{1}$$

and under the Reynolds analogy assumption with $Pr = 1$,

$$h_x = 1/2 c_{f,x} \frac{U \cdot k}{\nu} \tag{2}$$

For the flat-plate turbulent boundary-layer case and for Reynolds numbers up to about 5×10^6, Eqs. (1) and (2) underestimate the actual heat transfer coefficient by about 15% (Ref. 10). According to Eq. (2), the local heat transfer coefficient is directly proportional to the local skin-friction coefficient. Since through transition from laminar to turbulent regime the skin-friction coefficient increases shaply, as shown in Fig. 2, by Reynolds analogy the heat transfer coefficient also increases in a similar way. Thus, under increasing temperature flow conditions, a step increase in the wall temperature should be seen on the thermogram at the transition location, due to the change in convective conditions above the surface.

Invoking again the Reynolds analogy, the leading-edge area of the airfoil is expected to experience relatively high heating rates, as long as the flow remains locally attached. This happens regardless of whether or not the boundary-layer flow is laminar or turbulent. Referring to the flat-plate model for an explanation, both the local heat transfer and the friction coefficients vary as Re_x^{-n}, with n being 0.5 in the laminar case and 0.2 in the turbulent case. For very low local Reynolds numbers, as is the case in the leading-edge area, both the heat transfer and the friction coefficients will take relatively high values, enhancing the local heat transfer.

In the case of separated flow the behavior of the convective heat transfer ceases to be easily predictable. In such a flow there are regions of high- and low-intensity heat transfer, all depending on the location, size, and strength of the vortices in the recirculation zone. A visual impression about the intensity and variation of the turbulent mixing in such a flow can be obtained from Schlichting (Ref. 11, p. 37, Fig. 2.19) or by watching one of Prandtl's flow visualization films.[12] The determination of guidelines for flow separation detection is not a straightforward task as in the case of transition. At this point further elaboration on the subject is relegated to the Discussion section.

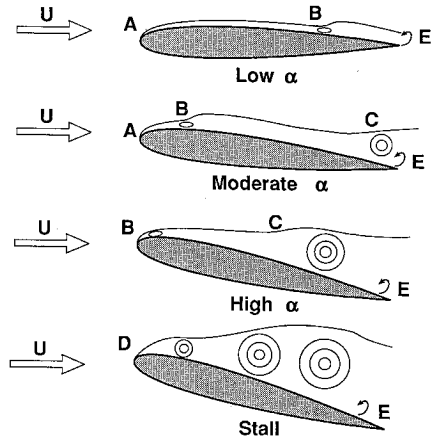

Fig. 2 Viscous flow regimes over upper surface of NACA 0012 airfoil.

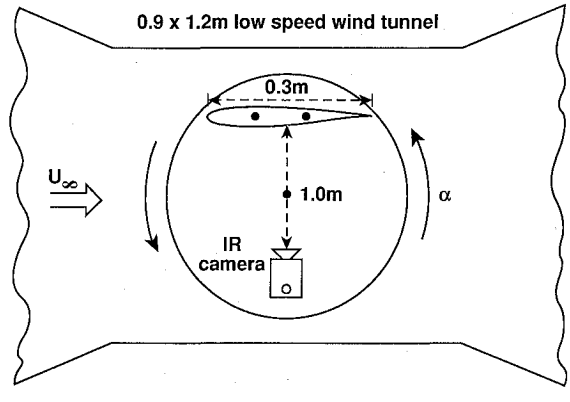

Fig. 3 Schematic top view of the IR imaging camera and airfoil mounting used for the wind-tunnel boundary-layer flow studies.

Wind-Tunnel Setup

The experimental setup was mounted on a turning table in a low-speed closed-circuit wind tunnel, with a test section of 0.9×1.2 m^2. The turbulence level of that wind tunnel was measured with a single hot-wire probe to be 0.7%. As shown in Fig. 3, this setup comprised a vertical NACA 0012 airfoil, mounted diametrically opposed to the IR imaging camera. As the table rotated around its center, the airfoil angle of attack was changed, but the camera remained in a fixed perpendicular position relative to the airfoil chord. The wind tunnel does not possess any means for cooling; therefore, the air continuously heats during operation. As a result, the airfoil in the test section is in turn heated by the air, and generally speaking its mean surface temperature is steadily rising. One benefit deriving from this situation is that the transition demarcation line, appearing on the airfoil thermograms, is greatly enhanced.

The airfoil was made of wood, had a chord of 0.305 m, an aspect ratio of 1.5, and was clamped between two end plates to reduce the three-dimensional flow effects of the tips. At zero angle of attack the airfoil was 10 cm away from the wind-tunnel side wall, and the camera was similarly spaced near the

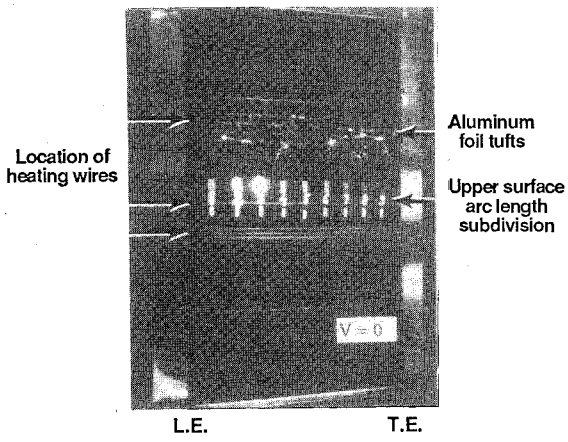

Fig. 4 NACA 0012 airfoil with aluminum foil tufts in still air.

opposite wall. Although this arrangement did affect the airflow around the airfoil (by wall proximity), the basic objective of the experiment, to study the signature of the boundary-layer behavior by IR imaging of the surface, was not hampered. The observations are reported as they were made, without accounting for the wall proximity. To eliminate any possible spurious reflections to the camera, the wood airfoil was covered with 0.152-mm-thick black matte paper. Figure 4 is a photograph displaying the following features of the airfoil:

1) Decimal subdivision of the upper surface arc length (herein referred to as s) was provided, where the lower and the upper divisions were marked with highly reflective silver paint and ultrafine gold leaf, respectively, to be visible on the IR imaging system display. A posteriori, it was concluded (see Fig. 6) that both the silver paint and the gold leaf markings could be observed equally well. Since the silver paint is easier to apply, it may be considered as the preferable choice.

2) Above the arc subdivisions, four rows of aluminum foil tufts 0.0254 mm thick and 2 mm wide, observable both visually and with the IR imaging system, were threaded through the paper in increments of one-tenth of the surface arc length ($0.1s$).

3) The airfoil surface was electrically warmed at discrete spanwise locations with a 0.127-mm constantan wire that had been wrapped chordwise around the airfoil underneath the black paper in the following locations: at the arc markings and at the tufts locations, to enhance their observability with the IR imaging camera by providing a low-temperature, low-emittance target against a high-temperature, high-emittance background; and below the arc markings, to allow tracking the boundary-layer development through chordwise temperature measurements on a smooth, uncontaminated airfoil surface.

The chordwise run of the heating wires is marked in Fig. 4 by pencil on the black paper. The uppermost and lowest lines demarcate the field of view of the IR imaging camera. The idea to use substrate heating was suggested by the encouraging results obtained earlier with this method in observing the signature of laminar boundary-layer development over a flat plate by computerized analysis of thermograms.[13] In the present case, the intent was to extract temperature differences from thermograms taken at different angles of attack in order to track changes in the boundary-layer behavior induced by increasing airfoil incidence. It was later realized that this attempt had to be dropped because of the nonlinear and uncontrollable heating of the air in the closed-circuit wind tunnel at initial rates of 1.2 K/min.

The imaging system used in this investigation was able to detect IR radiation in the 3.5- and 5.6-μ shortwave band. The

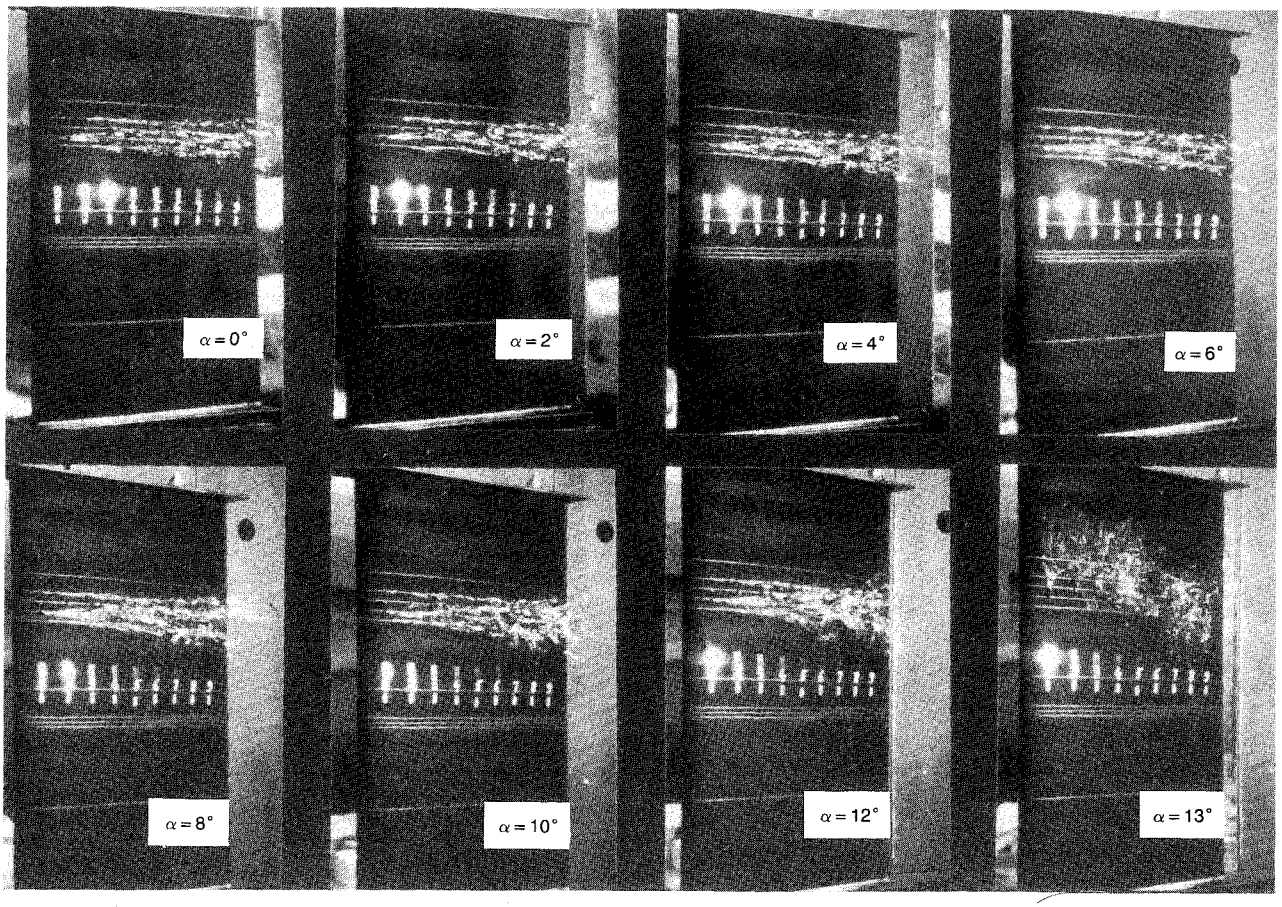

Fig. 5 NACA 0012 airfoil with aluminum foil tufts at various angles of attack. Re_c = 370,000, in wall proximity. Photographs were taken with 35-mm SLR camera. Air flows from left to right.

basic system consisted of the scanner and a black and white display unit. The objective lens chosen for this experiment has a field of view of 20 deg, which at 1 m distance covers an area of 0.3×0.3 m^2. In the normal mode the system assigns gradually lighter shades of grey to increasing temperatures of the object being scanned. However, in the experiments reported here the display unit was set for the inverted mode, which produces darker shades for higher surface temperatures. This choice was dictated by the fact that the tufts' status can be better seen in the inverted mode than in the normal mode. The system temperature range of measurement varies between 253 and 1123 K, but manual tuning has to be done at each of the nine available subranges to get sharp thermogram images of the target.

Description of the Experiment

The airfoil angle of attack was varied between 0 and 14 deg with an accuracy of ± 0.5 deg. Photographs of the airfoil surface were taken at each angle of attack with a 35-mm single lens reflex (SLR) camera, and of the IR imaging system display unit (oscilloscope face) using an instant camera. Later, the instant photos were reproduced using a 35-mm SLR camera. Pursuing this process, it was possible to confirm visually that the tufts behavior can be observed on the thermograms produced by the IR imaging system. Furthermore, the identification of the boundary-layer flow regimes based on the airfoil surface temperature distribution, as displayed on the thermograms, could be inferred from the tufts' behavior. This way, future investigations can rely solely on observations performed with the IR imaging system.

Results and Discussion

The visual observations documented in Fig. 5 show a sequence of the airfoil surface photographs taken with a 35-mm SLR camera for angles of attack varying between 0 and 13 deg. Figure 6 shows a similar sequence of pictures, this time as observed on the IR imaging system display. It is noticed that the tufts behavior is observable both visually and with the IR imaging camera, with the tufts being especially useful in indicating separation. On the negative side, the tufts themselves induce early transition and separation, but this phenomenon could be accounted for by observing on the IR imaging display both the tufts motion and the temperature signature on the surface.

The transition to turbulence and the separation of the boundary layer can be inferred from the tufts' motion. Three distinct types of behavior could be identified[14]:

1) tufts motionless and attached to the airfoil surface, pointing in the downstream flow direction, indicative of laminar flow;

2) tufts flutter, at ever-increasing rates chordwise and pointing downstream, indicative of turbulent flow; and

3) tufts reversal, sporadically or persistent, indicative of separated flow.

The pictures in Fig. 5 partially document the tufts' behavior as it could be observed visually. The word "partially" is used because continuous visual observation of the tufts offers more information than still photographs, especially with regard to the unsteady behavior of the flow. Even with this shortcoming, the sequence of photographs in Fig. 5 shows that, starting at $\alpha = 0$ deg, the turbulent boundary layer gradually expands upstream from the aft part of the airfoil with increasing angle of attack. At $\alpha = 6$ deg, turbulent separation is initiated, and subsequently the separation point also moves gradually upstream with increasing angle of attack. At $\alpha = 13$ deg, complete separation (stall) was observed. The complete separation occurred only after a few seconds once the airfoil was fixed in position at $\alpha = 13$ deg. As indicated by the tufts' behavior, the turbulent boundary-layer separation point was not stable with respect to time. Just after the separation had first been ob-

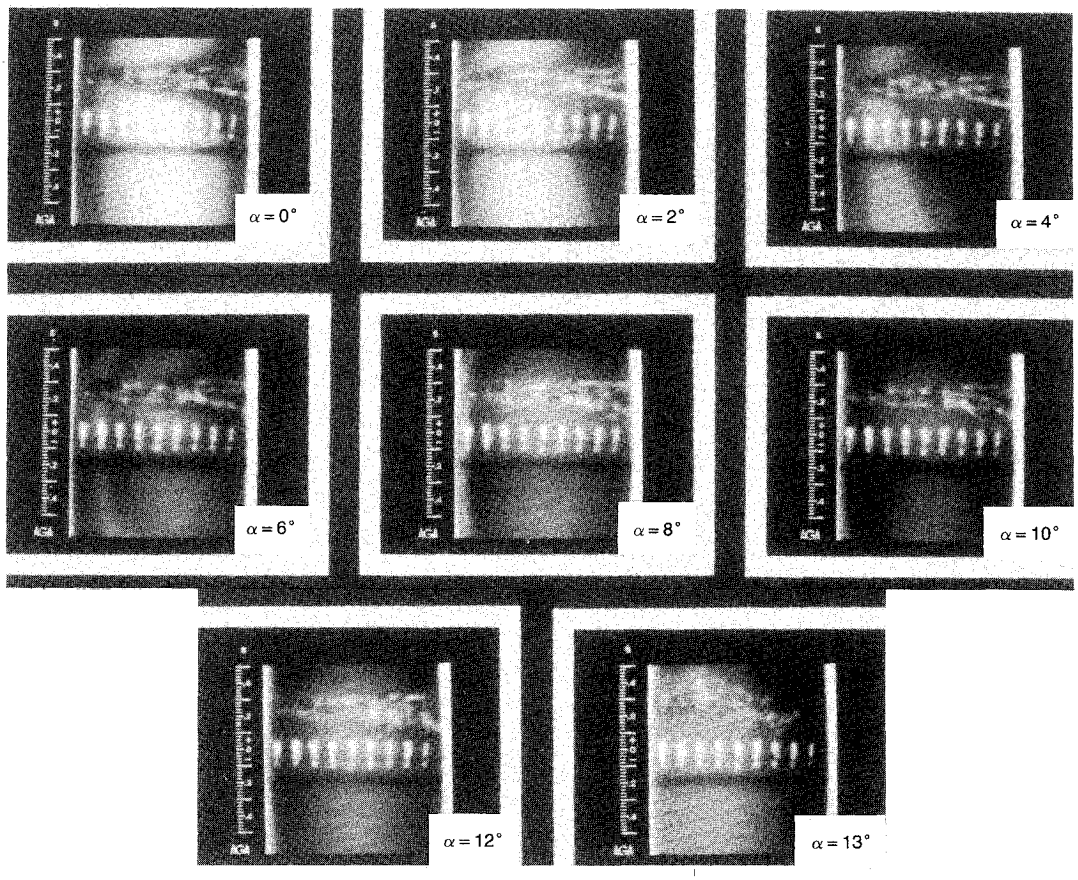

Fig. 6 NACA 0012 airfoil with aluminum foil tufts at various angles of attack. $Re_c = 375{,}000$, in wall proximity. Photographs of the infrared imaging display in inverted mode. Air flows from left to right.

served, at $\alpha = 6$ deg, separation line oscillations back and fourth over at least one-tenth of the surface could be observed. Just prior to the complete separation, at $\alpha = 13$ deg, these oscillations grew in frequency and amplitude and covered up to one-fourth of the surface.

For the present Reynolds number, stall at 13 deg is somewhat premature but could be expected considering the fact that the airfoil was placed near and spanwise parallel to the wind-tunnel wall. This assembly caused the airfoil to operate "in ground effect," thus increasing the effective angle of attack. In order to check the correctness of this assumption, the airfoil was temporarily moved to the center of the wind tunnel, where a few runs at the same Reynolds number repetitively indicated stall at 14 deg.

Before proceeding with review and discussion of the thermograms, the following points are recalled regarding their interpretation:

1) Each thermogram contains data indicative of the temperature distribution of the airfoil surface. Darker shades represent higher apparent temperatures (inverted mode).

2) The thermograms can be compared among themselves on a relative basis, to determine the extent of airfoil areas exposed to higher heating rates, as the angle of attack was changed.

3) The thermograms cannot be compared among themselves on an absolute basis, because the control unit of the imaging system was set anew for each thermogram, to get the clearest and sharpest image possible.

4) All of the thermograms were taken from the same relative position with respect to the airfoil, with the optical axis of the IR camera perpendicular to the airfoil chord. Therefore, apparent temperature differences between thermograms taken at different angles of attack should not be associated with directional emittance effects of the surface.

5) The airfoil surface directly underneath the tufts was electrically heated to enhance their observability with the IR system. Therefore, that area appears darker on the thermograms primarily due to its heating from beneath. The transition induced by the tufts can be unambiguously identified only when the characteristic wedge signature spreads out laterally, to the unheated area of the surface.

A close look at Fig. 6 provides the details that correlate the IR observations with the flow features. For this purpose the clean, undisturbed surface of the airfoil in the lower half of the thermograms is noted. The thermograms for $\alpha = 0$, 2, and 4 deg show two heated zones. The first is the effect of the convective heating under the laminar boundary-layer regime at the leading edge. The second, along the trailing edge and exhibiting a curved boundary shape, is due to the effect of convective heating under the turbulent boundary-layer regime. Just upstream of that darker curved shape is the region where the laminar to turbulent transition takes place. On the upper side of the thermograms the development of a "wedge" signature can be seen, attributed to early transition induced by the tufts. As the angle of attack is increased from 0 to 2 and from 2 to 4 deg, the transition region advances upstream, as expected. The next four thermograms from $\alpha = 6$–12 deg display the flow regime, where trailing-edge turbulent separation is indicated by the tufts. The separation vorticity is shed from that area,[11] and the resulting increased turbulence convects heat more efficiently from the freestream to the airfoil surface, causing a new darker (increased temperature) area to appear on the thermogram. The increased heat transfer to the wall associated with vorticity shedding in the separation zone is well documented in the case of cylinders in crossflow (Ref. 11, p. 312).

The thermogram taken at $\alpha = 6$ deg is particularly interesting because it captured the separation bubble at $0.15s$ as a lighter shade curved strip. Its extent there is about 10% of the upper surface. Since at the laminar separation line the first derivative of the velocity, $\partial u/\partial y$, is zero, so is $c_{f,x}$ and h_x. Therefore, the bubble appears as an area of lower temperatures due to the lower local convective heating of the surface. However, its observability depends on a very fine-tuning of the "thermal level" knob of the display unit, which may be detrimental to the capture of other features, making it hard to capture under arbitrary conditions. Thus, this thermogram displays the most interesting features related to IR imaging investigations of boundary-layer behavior over an airfoil: the increased heat transfer modes characteristic to the leading edge, transition, and vorticity shedding; and the decreased heat transfer characteristic of the laminar separation bubble.

The thermograms taken at $\alpha = 6$ and 8 deg show the transition front moving upstream. The thermogram taken at $\alpha = 8$ deg still displays the separation bubble as a lighter shaded area at the leading edge, slightly curving from the centerline outboard. As the angle of attack is further increased to $\alpha = 10$ and 12 deg, the stagnation point moves downward around the leading edge followed by the transition bubble, which gets almost entirely out of view of the IR camera. When the angle of atack is increased to $\alpha = 13$ deg, the stall angle is reached. The complete separation of the flow leaves on the airfoil surface a single area of higher heat transfer near the trailing edge, where the vorticity shedding occurs. Thus, the relative decrease in the heating rate at the leading-edge area can be associated with complete separation. This feature can be observed by comparing the thermograms taken at $\alpha = 12$ and 13 deg.

Guidelines for identification of the various boundary-layer regimes are given in Table 1, and the main findings of the experiments (visual and IR imaging observations) are summarized as follows:

1) $\alpha = 0$ deg: laminar flow up to $0.8s$ on the clean surface and tufts induced transition at $0.3s$;

2) $\alpha = 2$ deg: transition at $0.7s$ on the clean airfoil (lower part), tufts induced transition at $0.3s$, and tufts flutter at high amplitudes after $0.7s$;

3) $\alpha = 4$ deg: transition between 0.4 and $0.5s$ on the clean airfoil, tufts induced transition at $0.2s$, and tufts flutter at even higher amplitudes (compared to $\alpha = 2$ deg) after $0.7s$;

4) $\alpha = 6$ deg: transition at $0.2s$ on the clean airfoil, tufts induced transition at $0.2s$, turbulent separation seen on tufts at $0.8s$, and shedded vorticity signature on thermogram starting at $0.8s$;

5) $\alpha = 8$ deg: transition at $0.1s$ on all the airfoil, turbulent separation seen on tufts at $0.7s$, and shedded vorticity signature on thermogram starting at $0.8s$;

6) $\alpha = 10$ deg: fully developed turbulent flow all over the airfoil, turbulent separation seen on tufts at $0.6s$, and shedded vorticity signature on thermogram starting at 0.7–$0.8s$;

7) $\alpha = 12$ deg: "steady" separation seen on tufts at $0.5s$, with the separation point seen to move violently back and forth up to $0.3s$ and shedded vorticity signature on thermogram starting at 0.7–$0.8s$; and

8) $\alpha = 13$ deg: bubble burst, with complete separation occurring, and shedded vorticity signature on thermogram starting at 0.6–$0.7s$.

Taking an overall look at the thermograms of Fig. 6, it is seen that the contrast between darker and lighter shades (in the

Table 1 Regions of relatively high heat-transfer rates identified on infrared imaging thermograms of the NACA 0012 airfoil; Re_c = 375,000 (in "ground effect")

Incidence	Regions of increased heat transfer
Low (0–4 deg)[a]	1) leading-edge laminar; 2) transition
Medium (6–8 deg)	1) leading-edge laminar; 2) transition; 3) vorticity shedding
High (10–12 deg)	1) leading-edge turbulent; 2) vorticity shedding
Post-stall (13 deg and up)	1) vorticity shedding

[a]Indicative values.

inverted mode, higher and lower temperatures, respectively) tends to decrease with increasing angle of attack. Actually, that decrease in contrast is not due to the influence of change in angle of attack. Higher angle-of-attack thermograms were taken after longer operation periods of the tunnel, and the heating rate of the air was found to gradually decrease with time toward an eventual steady state. The overall luminosity level of the thermograms is, of course, determined by the "thermal level" adjustment of the IR imaging system.

Concluding the analysis of the sequence of thermograms presented in Fig. 6, it is underlined that the surface temperature information contained in each individual thermogram is not sufficient for a meaningful interpretation in itself. For example, the thermogram taken at 10-deg angle of attack can be ambiguously interpreted as indicating laminar flow with transition to turbulent flow at $0.7s$, the actual case being transition to turbulent flow near the leading edge and separation at $0.7s$ (the tufts indicating the separation onset at $0.6s$). Hence, it is a whole sequence of thermograms, rather than a single one, taken from 0-deg angle of attack up to separation that has to be examined all together in order to extract the surface temperature information that elucidates the changes in boundary-layer flow.

Summary

Transition and separation surface signature studies done by IR imaging showed that each type of boundary-layer flow regime can be associated with a region of relatively high heat transfer, identifiable on thermograms as a marked change in the airfoil surface temperature. At low angles of attack, where the flow is fully attached, there are two such zones: the first associated with laminar flow at the leading edge, and the second, further downstream, with transition to turbulence. As the angle of attack is increased, turbulent separation occurs near the trailing edge and a third region appears, indicative of shedded vorticity. With increasing incidence, the transition moves very near to the trailing edge; hence, the region associated with the leading-edge laminar influence disappears, leaving only two such regions: that associated with the transition to turbulence at the leading edge and that associated with the shedded vorticity. As the incidence is increased beyond the stall angle of attack, there remains only one region of marked increase in surface temperature: that associated with the shedded vorticity.

The development of tufts observable with the IR imaging camera enhances the versatility of this tool in aerodynamic research, due to the capability to perform temperature measurements and to visualize the flow behavior simultaneously.

Acknowledgment

This research was partially supported by NASA Langley Research Center Grant NAG 1-735.

References

[1]Quast, A., "Detection of Transition by Infrared Image Technique," *Proceedings of the 12th International Congress on Instrumentation in Aerospace Simulation Facilities (ICIASF 87),* IEEE Publ. 87CH2449-7, 1987, pp. 125–139.

[2]Horstmann, K. H., Quast, A., and Redeker, G., "Flight and Wind-Tunnel Investigations on Boundary-Layer Transition," *Journal of Aircraft*, Vol. 27, No. 2, 1990, pp. 146–150.

[3]Schmitt, R. L., and Chanetz, B. P., "Experimental Investigation of Three Dimensional Separation on an Ellipsoid-Cylinder Body at Incidence," AIAA Paper 85-1686, July 1985.

[4]Brandon, J. M., Manuel, G. S., Wright, R. E., and Holmes, B. J., "In-Flight Flow Visualization Using Infrared Imaging," AIAA Paper 88-2111, May 1988.

[5]Monti, R., and Zuppardi, G., "Computerized Thermographic Technique for the Detection of Boundary Layer Separation," *Aerodynamic Data Accuracy and Quality: Requirements and Capabilities in Wind Tunnel Testing*, AGARD CP-423, 1987, Chap. 30.

[6]Carlomagno, G. M., Deluca, L., Buresti, G., and Lombardi, G., "Characterization of Boundary Layer Conditions in Wind Tunnel Tests through IR Thermography Imaging," *Applications of Infrared Technology*, Society of Photo-Optical Instrumentation Engineers, Bellingham, WA, Vol. 918, 1988, pp. 23–29.

[7]McCullough, G. B., and Gault, D. E., "Examples of Three Representative Types of Airfoil-Section Stall at Low Speed," NACA TN-2502, Sept. 1951.

[8]Thwaites, B. (ed.), *Incompressible Aerodynamics,* Dover, New York, 1987, pp. 200–205.

[9]Gauffre, G., "Detection de la Transition Laminaire Turbulent par Thermographie Infrarouge," *La Recherche Aérospatiale*, No. 2, March–April 1988, pp. 11–22 (also English translation).

[10]Kays, W. M., and Crawford, M. E., *Convective Heat and Mass Transfer*, McGraw-Hill, New York, 1980, pp. 175, 212, 213.

[11]Schlichting, H., *Boundary Layer Theory*, McGraw-Hill, New York, 1979.

[12]Prandtl, L., "Generation of Circulation and Lift for an Airfoil," Experiments done at Gottingen, 1909, National Committee for Fluid Mechanics Films, Film Roll FM-10, edited by A. H. Shapiro and R. Bergman, Aug. 1962.

[13]Gartenberg, E., Roberts, A. S., Jr., and McRee, G. J., "Aerodynamic Investigation by Infrared Imaging," *Proceedings of the 6th Applied Aerodynamics Conference*, AIAA, New York, 1988, pp. 121–128.

[14]Carr, L. W., McAlister, K. W., and McCroskey, W. J., "Analysis of the Development of Dynamic Stall Based on Oscillating Airfoil Experiments," NASA TN D-8382, Jan. 1977, p. 9.